Identification of Joint Stiffness Matrix Using a Decomposition Technique

Matthew S. Young – Graduate Research Assistant
Presently Research Scientist, Battelle Memorial Institute

Mayank Tiwari - Post Doctoral Researcher
Presently Staff Engineer, GE Global Research

Rajendra Singh – Professor

The Ohio State University
Department of Mechanical Engineering
Acoustics and Dynamics Laboratory
Center for Automotive Research
201 West 19th Avenue
Columbus, Ohio 43210-1107, USA

ABSTRACT

Properties of joints in an assembly play a significant role in the static and dynamic response of the assembly. However, it is difficult to analytically model joints, especially the off-diagonal terms. In this paper, the dynamic stiffness matrix of an assembly is extracted using frequency response functions (FRF) of two individual components and the joined assembly of these components. It is shown that each component may be described using FRF's from experimental, or finite element model, or analytical data. The assembly FRF is obtained experimentally. This decomposition method applies the dynamic compliance technique to produce a dynamic stiffness matrix of dimension 2 including shear, rotation, and cross-coupling terms. The technique is tested on an experimental assembly consisting of two rigid components joined by a thin compliant beam that is integral to the assembly. The stiffness matrix resulting from the decomposition procedure is compared with values obtained from applying Euler's beam theory to the beam joint and compared with the decomposition of FRF's obtained from a finite element model of the same system. Future applications of this technique are considered.

Table of Nomenclature

Boldface	Vectors and matrices are indicated with boldface
A, B	Individual assembly components
F	Force excitation amplitude (complex valued)
H	Dynamic compliance of an assembly
J	Mass moment of inertia of a component
K	Stiffness of joint
l_j	Joint length
l	Component length

Nomenclature Continued

m	mass
M	Mass matrix
Q	Moment excitation amplitude (complex valued)
D(ω)	Assembly dynamic stiffness matrix
X,Y	Translational displacement amplitude (complex valued)
y	Static displacement
α, β, γ	Dynamic compliance matrices of components A, B, and C respectively
θ	Rotational displacement amplitude (complex valued)
ω	Frequency (rad/s)
K_d	Dynamic stiffness of joint
K_s	Static Stiffness
i	Location of displacement measurement
j	Location of excitation
J	Joint
E	Modulus of elasticity
1,2,3…	Component location
EXP	Experiment based data
FEM	Finite element model
LPD	Lumped parameter model based on Euler's beam theory

INTRODUCTION

Noise, vibration and harshness characteristics of sheet metal structures such as vehicle frames are significantly influenced by welded or adhesive joints and interfaces. In automotive applications, relatively compliant structures are often inter-connected by many spot welds or glued connections. In some cases, these connections may contribute up to 60% of an assembly's flexibility and 90% of its damping [1]. Wolf and Kamal [2] found that local compliances in automotive frames associated with structural joints are significant. They recommended the addition of static rotational stiffness elements in linear finite elements models, since such elements effectively model the slope discontinuities associated with structural joints. Doing this improved the accuracy of their models by as much as 50 %.

The joint mechanics problem is of interest not only from the structural acoustics standpoint, but also from standpoint of static or fatigue analyses, impact strength and durability. In automotive systems, engineers have found the following noise and vibration control problems that are controlled by joints: a. Variation in elastic modes of deformation and their couplings with acoustic cavities, b. Influence of the joining process on perceived vehicle quality. The chief objective of this article is to develop a practical and repeatable laboratory technique for extracting joint properties from compliant structures with the ultimate goal of predicting assembly behavior.

In this article, a decomposition procedure is proposed based on frequency domain component synthesis to extract the stiffness matrix of an elastic element that joins two rigid structures. The proposed methodology, as shown in Figure 1, is illustrated via analytical, computational and experimental techniques.

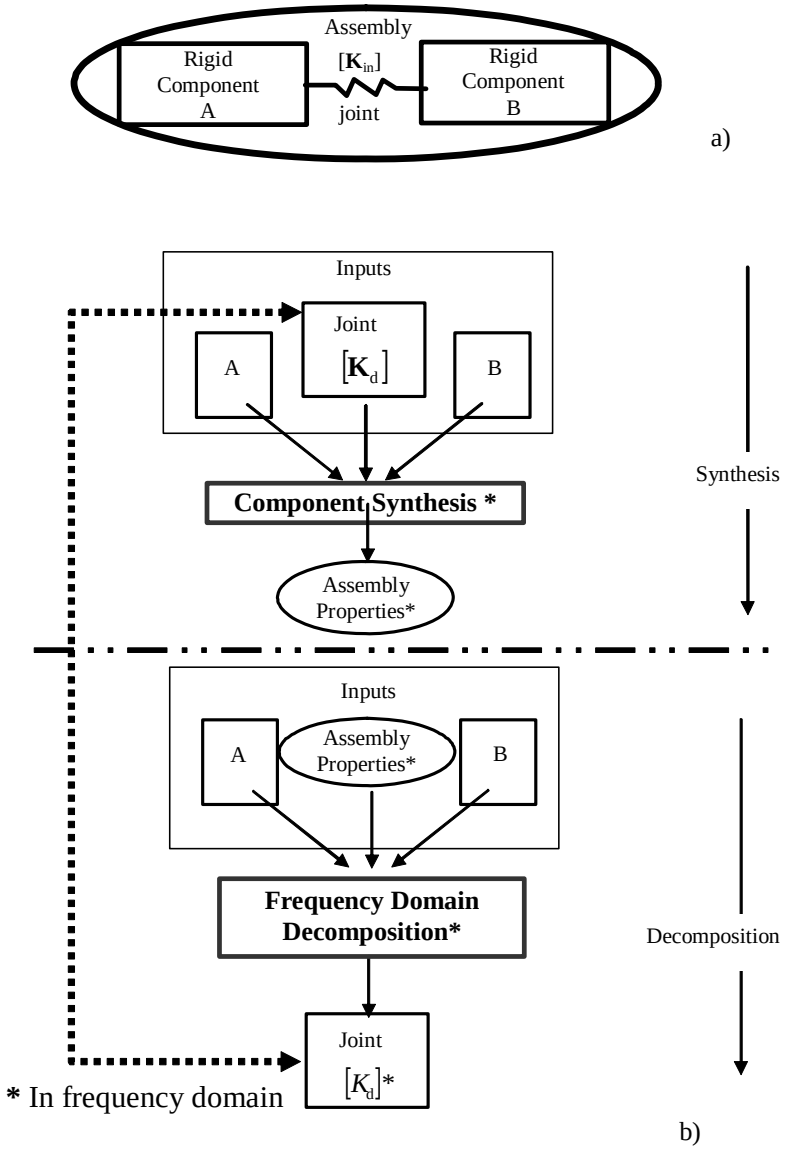

Fig. 1. Summary of the proposed method. a) An assembly consisting of two rigid components, A and B, and a joint of stiffness matrix K_d. b) Component synthesis and decomposition procedures.

LITERATURE REVIEW

Some effort has gone into developing experimental techniques for extracting joint stiffness values from assemblies. Two basic techniques have been proposed in the literature. The first technique relies on static stiffness and requires deformation measurements at the joint location given a known static force [3]. However, it has been shown that static and dynamic stiffness values may not match. The second strategy identifies joint properties based on measured vibration data of a joined assembly, but most of these efforts are limited to the extraction of direct properties of the joint and few describe the measurement of rotational components of the joint matrix. For instance, Wang and Liou [4] proposed a method in which one of two joined components is rigidly fixed while the second one is unconstrained. Selected frequency response function (FRF) measurements are made on the unconstrained component before and after joining. Measured data are then processed using theory to backtrack the joint properties. This method is useful for laboratory structures with discrete one-dimensional joints, but the cross properties of the joint are still not estimated by this technique. Ren and Beards [2] used a similar

method while suggesting techniques for improving the calculation accuracy based on the relative compliance of the joint in question, matrix conditioning and experimental signal errors. This method appears to work well for multi-dimensional beam systems when simulated using finite elements. Ren and Beards [5,6] developed theoretical and experimental methods to further improve the accuracy of FRF identification methods and to consider inaccessible joints. In these studies, the response of the rotational degree of freedom is not taken into consideration. The difficulties associated with experimental moment mobility measurements are addressed by Juanxin and Mak [7] who demonstrate improvements in a moment-only excitation system based on minimizing its force impedance, while Ivarsson and Sanderson [8] consider force and moment excitation simultaneously in multi-input multi-output experiments.

Liu and Ewins [9,10] have presented a theoretical method for determining joint mass, damping and stiffness matrices by measuring FRF's at certain locations that are not necessarily at the joint-component boundary. The partitioning algorithm suggested in this work results in a better conditioning of the FRF matrix and reduces computational time. Chen et al. [11] have proposed a complex mode method to extract mass, stiffness and damping matrices from measured FRF's. Chou and Tsai [12] have proposed a bolt joint identification method using measured FRF's. The advantage of this method is that the location of the FRF measurement is independent from the joint location; however the rotational stiffness issue has not been dealt with in this work. Measurement of rotational displacements is difficult but it is vital to developing accurate models of assembled structures [1]. Liu and Ewins [13] have described a quantitative method to estimate errors due to neglecting rotational displacements. Some rotational measurements have been attempted by Stainbridge and Ewins [14] and Mitchell et al. [15] with a laser Doppler vibrometer. Yoshimura and Hosoya [16] evolved a synthesis procedure employing harmonic moment excitation that extracted the FRF's associated with rotational motion. The application of a laser Doppler vibrometer to measure rotational compliance was not used in this paper, but could be relevant to future work in this vein.

The effect of joint stiffness on the natural frequencies of an assembly has been theoretically and experimentally shown by Singh et al. [17]. In this work, generic sheet metal structures such as 'L', 'T', and 'U' shapes were built using different kinds of welded, riveted and adhesive joints. Three distinct regimes were identified in the natural frequency-joint stiffness curve, which is 'S' shaped. The assembly natural frequency has greatest sensitivity to a specific joint stiffness value in the middle part of this 'S' curve. Liu et al. [18] describe the use of translational and rotational stiffness components to represent line and tack welds in finite element models.

PROBLEM FORMULATION

This paper focuses on obtaining the multi-dimensional properties of a joint, especially the off-diagonal terms of the stiffness matrix. Our study also addresses the issue of experimental measurement of rotational displacement and rotational stiffness terms. This technique provides the option of combining experimental, theoretical and computational data when necessary.

The scope of this study is limited to the first few vibration modes of an assembly that consists of two rigid components (A and B) joined by a flexible beam (Figure 2). The beam-joint was chosen because its lumped static stiffness matrix ($\mathbf{K_s}$) can be derived from Euler's beam theory and used for verification of the extracted stiffness matrix values. Table 1 records the dimensions of the test specimen.

Experimental results are compared with two mathematical models of the same system. The first one is a lumped parameter analytical model referred to as LPD (for "lumped model"), which employs a static stiffness matrix based on Euler beam theory. The second model is a 3-D finite element model (referred to as FEM) that is constructed using solid brick elements.

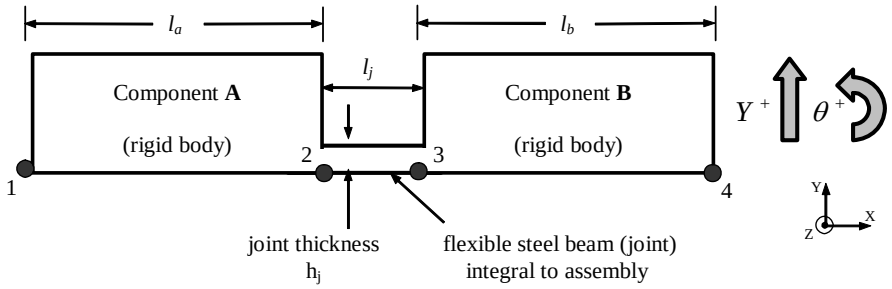

Fig. 2. Example cases. Refer to Table 1 for component dimensions.

Component	Joint Dimensions		
	Length (l)	Thickness (h)	Depth (d)
Integral Steel Beam	13 mm	1.2 mm	13 mm
Rigid body A	25 mm	75 mm	25 mm
Rigid body B	25 mm	75 mm	25 mm

Table 1. Dimensions of components shown in Figure 2.

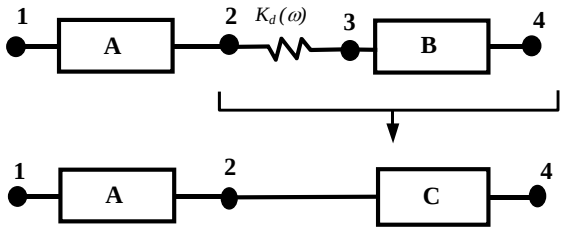

Fig. 3. Compliant joint of dynamic stiffness $K_d(\omega)$ between two rigid components. ($K_d(\omega)$ shown is a multi-directional spring.) Here, an equivalent component C may be substituted for the joint and component B.

COMPONENT SYNTHESIS METHOD

Lumped Model of Joint

The mobility technique [19-23] is most often used to synthesize the dynamic behavior of an assembly given FRF's of individual components and the stiffness of associated joints. Conversely, one may adopt the inverse synthesis or decomposition process to extract the properties of joints as suggested in Figure 1. One advantage of this method is its application to components under free-free boundary conditions, which are easiest to simulate experimentally. The simplest illustration includes two rigid components, A and B, connected with a one-dimensional joint element of dynamic stiffness, $K_d(\omega)$, as indicated in Figure 3. The extracted stiffness, which is the dynamic stiffness, may include joint mass M_J and damping C_J terms as well as static stiffness K_s terms:

$$K_d(\omega) = -\omega^2 M_J + i\omega C_J + K_s \quad (1)$$

In this paper, the mass and damping terms of K_d are assumed negligible due to the assembly geometry chosen. Displacement and dynamic compliance FRF's are used rather than velocity and mobility. The displacement amplitude Y_i at any given point is

$$Y_i(\omega) = F_i H_{ii} + F_j H_{ij} \quad (2)$$

Where F_i and F_j are the amplitudes of harmonic forces applied at points '*i* ' and '*j* ' respectively. The driving-point compliance is H_{ii} and cross-point compliance, given excitation at *j* is H_{ij}. All variables in equation (2) are complex-valued and functions of frequency with the ubiquitous $e^{i\omega t}$ term dropped for the sake of brevity. The goal of synthesis is to mathematically join components A and B together and determine the response at point *4* for a given excitation at point *1* (Figure 3). When examining component A by itself in the horizontal direction only, the compliance matrix [α] terms include the following:

$$Y_1 = \alpha_{11}F_1 + \alpha_{12}F_2 \; ; \qquad Y_2 = \alpha_{21}F_1 + \alpha_{22}F_2 \quad (3a,b)$$

$$\alpha_{21} = Y_2 / F_1 ; \qquad \alpha_{11} = Y_1 / F_1 ; \qquad \text{given } F_2 = 0 \quad (4)$$

$$\alpha_{12} = Y_1 / F_2 ; \qquad \alpha_{22} = Y_2 / F_2 ; \qquad \text{given } F_1 = 0 \quad (5)$$

Likewise, for component B, one may define the elements of the β matrix:

$$Y_3 = \beta_{33}F_3 + \beta_{34}F_4 ; \qquad Y_4 = \beta_{43}F_3 + \beta_{44}F_4 \quad (6a,b)$$

$$\beta_{34} = Y_3 / F_4 \; ; \qquad \beta_{44} = Y_4 / F_4 ; \qquad \text{given } F_3 = 0 \quad (7)$$

$$\beta_{43} = Y_4 / F_3 \; ; \qquad \beta_{33} = Y_3 / F_3 ; \qquad \text{given } F_4 = 0 \quad (8)$$

Rigid Joint Between Components A and B

Assume that the joint in Figure 2 is a single degree of freedom spring, massless and containing no dissipative property, such as the simplified one shown in Figure 3. Without dissipative or mass components, $K_d(\omega) = K_s$. If the joint is assumed to be rigid, then the conditions of compatibility and equilibrium between the two components are,

$$Y_2 = Y_3 \;\; ; \;\; F_2 + F_3 = 0 \quad (9a,b)$$

Equations (3a,b) through (9) could now be combined to synthesize the assembly as:

$$\begin{Bmatrix} Y_1 \\ Y_4 \end{Bmatrix} = \begin{bmatrix} (\alpha_{11} - \alpha_{12}(\alpha_{22} + \beta_{33})^{-1}\alpha_{21}) & (\alpha_{12}(\alpha_{22} + \beta_{33})^{-1}\beta_{34}) \\ (\beta_{43}(\alpha_{22} + \beta_{33})^{-1}\alpha_{21}) & -(\beta_{43}(\alpha_{22} + \beta_{33})^{-1}(\beta_{34} + \beta_{44})) \end{bmatrix} \begin{Bmatrix} F_1 \\ F_4 \end{Bmatrix} \quad (10)$$

From this matrix equation, the cross compliance of the assembled structure can be found based on the compliance of the individual components. For example, one may relate Y_4 to F_1 as:

$$Y_4 = \beta_{43}(\alpha_{22} + \beta_{33})^{-1}\alpha_{21}F_1 \quad (11)$$

Compliant Joint Between Components A and B

The joint is once again made flexible with a dynamic stiffness $K_d(\omega)$. As illustrated in Figure 3, an equivalent component C of compliance γ may be substituted for the combination of the beam joint and component B. This substitution in equation (10) returns the system to the rigidly joined ($K_s \to \infty$) system of Figure 3 with the following relationship:

$$Y_4 = \gamma_{42}(\alpha_{22} + \gamma_{22})^{-1}\alpha_{21}F_1 \quad (12)$$

The compliance γ terms are related to β and K_d and from this the stiffness $K_d(\omega)$ can be extracted as:

$$K_d(\omega) = \left(\alpha_{21}\frac{1}{H_{41}}\beta_{43} - \alpha_{22} - \beta_{33}\right)^{-1} \quad (13)$$

Each variable in equation (13) is complex valued and spectrally-varying including K_d itself. For the multi-dimensional case, stiffness becomes a matrix as shown below; variables shown in bold are matrices or vectors.

$$\mathbf{K}_d(\omega) = \left(\boldsymbol{\alpha}_{21}\mathbf{H}_{41}{}^{-1}\boldsymbol{\beta}_{43} - \boldsymbol{\alpha}_{22} - \boldsymbol{\beta}_{33}\right)^{-1} \quad (14)$$

ANALYTICAL CALCULATIONS

Lumped Parameter Model (LPD)

Components A and B can be modeled as rigid bodies since the first flexural mode does not occur until 12 kHz which is well beyond the 500 Hz experimental scope of this study. Using Euler's beam theory, a four DOF model for the static stiffness matrix is developed to confirm the applicability of the component decomposition method. This simple model should also provide insight into the matrix algebra involved in the synthesis solution. The 2 DOF (shear and rotation) mass matrices (M_A, M_B) for A and B are first obtained by keeping the reference axes about points 2 and 3 respectively (Figure 2). Using the sign convention of Figure 2, we obtain:

$$\mathbf{M}_A = \begin{bmatrix} m_A & -(l_A/2)m_A \\ -(l_A/2)m_A & J_{A2} \end{bmatrix} \quad (15)$$

$$\mathbf{M}_B = \begin{bmatrix} m_B & (l_B/2)m_B \\ (l_B/2)m_B & J_{B3} \end{bmatrix} \quad (16)$$

where: m_A, m_B = mass of component A, B
J_{A2}, J_{B3} = mass moment of components A, B about points 2, 3
l_A, l_B = length of component A, B

These component mass matrices are used to create the $\boldsymbol{\alpha}$ and $\boldsymbol{\beta}$ terms of equation (14). To determine the assembly cross-point compliance term $\mathbf{H}_{41}$, the mass and stiffness matrices of an assembled system must be determined. The assembly mass **M** and static stiffness $\mathbf{K}_s$ matrices are given in equations (17 & 18). $\mathbf{K}_s$ is based on Euler's beam theory as detailed in Thomson [24].

$$\mathbf{M} = \begin{bmatrix} m_A & -\frac{l_A}{2}m_A & 0 & 0 \\ -\frac{l_A}{2}m_A & J_{A2} & 0 & 0 \\ 0 & 0 & m_B & \frac{l_B}{2}m_B \\ 0 & 0 & \frac{l_B}{2}m_B & J_{B3} \end{bmatrix} \quad (17)$$

$$\mathbf{K}_{Euler} = \frac{EI}{l_j^{\,3}} \begin{bmatrix} 12 & 6l_j & -12 & 6l_j \\ 6l_j & 4l_j^{\,2} & -6l_j & 2l_j^{\,2} \\ -12 & -6l_j & 12 & -6l_j \\ 6l_j & 2l_j^{\,2} & -6l_j & 4l_j^{\,2} \end{bmatrix} \quad (18)$$

where: E = modulus of elasticity of the beam
I = area moment of inertia of the beam
l_j = length of the joint

One may express equation (18) as follows where the physical behavior of the cross-stiffness terms $k_{F\theta}$ and k_{QY} can be visualized by loading the free end of a cantilevered beam. Here, a concentrated shear force (F) acting on the beam creates not only translational deflection (Y) with stiffness k_{FY}, but also a rotation (θ) with stiffness $k_{F\theta}$. Similarly, a moment (Q) acting on the end of a cantilevered beam would create rotational deflection with stiffness $k_{Q\theta}$ along with stiffness k_{QY} corresponding to translational deflection.

$$\mathbf{K}_S = \begin{bmatrix} k_{FY} & k_{F\theta} & -k_{FY} & k_{F\theta} \\ k_{QY} & k_{Q\theta} & (k_{QY} - l_j k_{FY}) & (-k_{Q\theta} + l_j k_{F\theta}) \\ -k_{FY} & -k_{F\theta} & k_{FY} & -k_{F\theta} \\ (-k_{QY} + l_j k_{FY}) & (-k_{Q\theta} + l_j k_{F\theta}) & -k_{QY} & k_{Q\theta} \end{bmatrix} \quad (19)$$

Assuming minimal damping for the one-piece steel test assembly, we obtain $\mathbf{M}\ddot{\mathbf{X}} + \mathbf{K}_s\mathbf{X} = \mathbf{0}$ as the governing set of equations where $\mathbf{X} = [\mathbf{Y_A}, \theta_A, \mathbf{Y}_B, \theta_B]^T$ and superscript T implies a transpose. The lumped model has four degrees of freedom since both A and B can independently translate and rotate.

The finite element model serves as an additional comparison to the experimental and lumped model results. The FEM model (created using ANSYS software [25]) contains only solid brick elements. The components are placed 13 mm apart as in the experiment. The beam joint is attached to the components rigidly and the elastic beam itself is divided into many elements which allow it to describe many more modes than the lumped model.

Verification by Modal Analysis

Computed and measured Eigen values are compared in Tables 2 and 3 and show a strong agreement between experimental, analytical and finite element results. Note that the free-free 4 DOF system lumped model does not calculate the third mode, since the first two modes at 0 Hz describe rigid body translation and rotation. The mode shapes related to these natural frequencies are identical. Table 3 illustrates the mode shapes obtained from

FEM. Mode 1 of Figure 4 and Table 3 results from an interaction between the component inertias and the rotational stiffness and cross-stiffness elements of K_s. Mode 2 is related to the shear stiffness and cross stiffness elements of K_s. Thus, the frequency range only up to the second natural frequency will be considered in this study, because the higher modes are related to the inertia of the beam joint and do not apply to most practical joints.

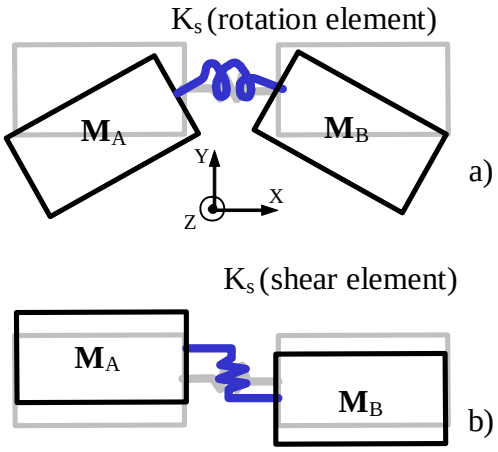

Fig. 4. Simplified illustration of lumped model. a) Mode 1, b) Mode 2.

Method	Abbrev.	Mode 1 (Hz)	Mode 2 (Hz)	Mode 3 (Hz)
Lumped Parameter Model	LPD	67	502	N/A
Experiment	EXP	58	502	4,040
Finite Elements	FEM	57	474	4,077

Table 2. Comparison of observed natural frequencies.

Mode	Deformed Shape	Description
1	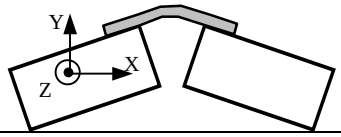	Dictated by beam rotational elements
2	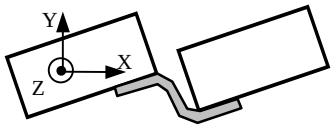	Controlled by the beam shear elements
3	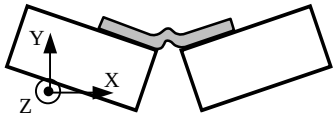	First elastic deformation mode of beam. (Not considered in this paper.)

Table 3. First three mode shapes (for both cases). Only modes in the X-Y plane are shown.

Simulation of Compliance Spectra

Compliance spectra of A and B and the cross-point compliance $\mathbf{H}_{41}$ of the assembly are required for the component synthesis calculation. Since A and B can be modeled as rigid bodies in this case, their driving point compliances at reference points (2 and 3) are:

$$\boldsymbol{\alpha}_{22} = \begin{bmatrix} Y_2/F_2 & Y_2/Q_2 \\ \theta_2/F_2 & \theta_2/Q_2 \end{bmatrix}_{\omega} = (-\omega^2 \mathbf{M}_A)^{-1} \begin{bmatrix} 1 & 0 \\ 0 & 1 \end{bmatrix} \tag{20}$$

$$\boldsymbol{\beta}_{33} = \begin{bmatrix} Y_3/F_3 & Y_3/Q_3 \\ \theta_3/F_3 & \theta_3/Q_3 \end{bmatrix}_{\omega} = (-\omega^2 \mathbf{M}_B)^{-1} \begin{bmatrix} 1 & 0 \\ 0 & 1 \end{bmatrix} \tag{21}$$

For cross-point compliance terms, the excitation or response must be transferred between component locations. The excitation for $\boldsymbol{\alpha}_{21}$ must be moved from reference point 2 to point 1. Here, F_2 can be transformed into the same force F_1 along with a moment Q_1 at location 1. Moment Q_2 can be transferred directly to Q_1 because the response due to a moment is irrespective of the point of application within a rigid body.

$$F_2 \Rightarrow \begin{cases} F_1 = F_2 \\ Q_1 = -l_A F_2 \end{cases}, \quad Q_2 \Rightarrow \begin{cases} F_1 = 0 \\ Q_1 = Q_2 \end{cases} \tag{22a,b}$$

The above transformation creates the following compliance matrix

$$\boldsymbol{\alpha}_{21} = \begin{bmatrix} Y_2/F_1 & Y_2/Q_1 \\ \theta_2/F_1 & \theta_2/Q_1 \end{bmatrix}_{\omega} = (-\omega^2 \mathbf{M}_A)^{-1} \begin{bmatrix} 1 & 0 \\ -l_A & 1 \end{bmatrix} \tag{23}$$

Similarly, $\boldsymbol{\beta}_{43}$ is given by the following

$$\boldsymbol{\beta}_{43} = \begin{bmatrix} Y_4 / F_3 & Y_4 / Q_3 \\ \theta_4 / F_3 & \theta_4 / Q_3 \end{bmatrix} = (\Gamma_{\text{mod}})^{-1} \begin{bmatrix} 1 & 0 \\ 0 & 1 \end{bmatrix} \tag{24}$$

where Γ is the transformed compliance matrix:

$$\Gamma_{\text{mod}} = \left(-\omega^2 \mathbf{M}_B\right) \begin{Bmatrix} Y_4 - l_B \theta_4 \\ \theta_4 \end{Bmatrix} \tag{25}$$

The dynamic response of an assembly described by the lumped model of Figure 3 is given by equations (26 & 27) in terms of the assembly's dynamic stiffness matrix **D**. Here, the joint stiffness matrix $\mathbf{K}_s$ is the Euler stiffness matrix (18) and **M** is the assembly mass matrix (17).

$$\mathbf{D}(\omega) \begin{Bmatrix} Y_2 \\ \theta_2 \\ Y_3 \\ \theta_3 \end{Bmatrix} = \begin{Bmatrix} F_2 \\ Q_2 \\ F_3 \\ Q_3 \end{Bmatrix} \tag{26}$$

$$\mathbf{D}(\omega) = -\omega^2 \mathbf{M} + \mathbf{K}_s \tag{27}$$

Since we are interested in $\mathbf{H}_{41,}$ the response point must be shifted from reference point 3 to 4 and the excitation point shifted from 2 to 1. The dynamic stiffness matrix **D**(ω) of the assembly in equation (26) is obtained by a coordinate transformation. In equation (26), replace Y_3 & θ_3 by Y_4 & θ_4 knowing that $Y_3 = Y_4 - l_B \theta_4$ and $\theta_3 = \theta_4$. Next, $\mathbf{H}_{41}$ can be extracted from equation (28) after partitioning the left hand side 4x2 matrix into two sub-matrices of 2x2

$$\begin{bmatrix} \mathbf{H}_{21} \\ \mathbf{H}_{41} \end{bmatrix} = \left[\mathbf{D}_{\text{mod}}(\omega)\right]^{-1} \begin{bmatrix} 1 & 0 \\ -l_A & 1 \\ 0 & 0 \\ 0 & 0 \end{bmatrix} \tag{28}$$

With $\mathbf{H}_{41}$ now determined, we have all the required arguments to calculate $\mathbf{K}_d$ (14). The $\boldsymbol{\alpha}_{21}$, $\boldsymbol{\alpha}_{22}$, $\boldsymbol{\beta}_{33}$, and $\boldsymbol{\beta}_{43}$ matrices, as described above are required for decomposition. These matrices will be used in both lumped and FEM models. The system mass **M** of equation (17) and $\mathbf{K}_s$ of equation 18) matrices will serve as inputs in the calculation of $\mathbf{H}_{41}$. To validate the method, after processing the compliance matrices through the decomposition equation (14), the resulting "output" stiffness matrix of the undamped joint, $\mathbf{K}_d(\omega)$, can be compared with the input static stiffness matrix $\mathbf{K}_{\text{Euler}}$ of equation 18. Each element of the $\boldsymbol{\alpha}$, $\boldsymbol{\beta}$ and $\mathbf{H}$ compliance matrices is a complex valued, discrete vector representing a narrow band frequency spectrum with $\Delta\omega$ resolution.

EXPERIMENTAL METHODOLOGY

Measurement of Compliance Matrices

Rotational stiffness elements are needed to accurately model an assembly [2, 13, 16], but the rotational motions are difficult to measure. To apply our technique to the estimation of rotational stiffness, a harmonic moment excitation of amplitude *Q* is applied and the corresponding rotational displacements are measured as shown in Figure 5. For measuring θ, two single-axis translational accelerometers are placed with a measured spacing *(l)* on a rigid surface [26], as illustrated in Figure 6a. The difference between the two complex valued acceleration amplitudes ($\ddot{Y}_i$ and $\ddot{Y}_j$) divided by *l* and integrated twice yields the rotational displacement amplitude. In frequency domain, the double integration yields the following:

$$\theta(\omega) = -(\ddot{Y}_j - \ddot{Y}_i)/\omega^2 l \qquad (29)$$

Moreover, in applying the moment excitation (*Q* = *F*d*), the impulsive force amplitude (*F*) is multiplied by its normal distance *(d)* from a reference point. Note that a force can be excited independently in this study, but a moment excitation is always coupled with a force. Exciting with both force and moment excitations and measuring both translation and rotation results in the following dynamic compliance and joint stiffness matrices, each of dimension 2.

$$\mathbf{H}_{ij}(\omega) = \begin{bmatrix} Y_i/F_j & Y_i/Q_j \\ \theta_i/F_j & \theta_i/Q_j \end{bmatrix}; \quad \mathbf{K}_{ij}(\omega) = \begin{bmatrix} F_j/Y_i & F_j/\theta_i \\ Q_j/Y_i & Q_j/\theta_i \end{bmatrix} \qquad (30\ a,b)$$

Free-free boundary conditions are used in this study since they can be more accurately simulated in experiments than any other boundary conditions. Here the assembly is suspended with very compliant supports. The compliance matrix $\boldsymbol{\alpha}_{21}$ is a 2 x 2 matrix where each element of the matrix is a frequency response function as shown by equation (31). Sign conventions and the experimental setup for determining this matrix are shown in Figure 6b.

$$\boldsymbol{\alpha}_{21}(\omega) = \begin{bmatrix} Y_2/F_1 & Y_2/Q_1 \\ \theta_2/F_1 & \theta_2/Q_1 \end{bmatrix}_\omega \qquad (31)$$

The following FRF's for component A can be directly measured: (Y_1/F_1), (Y_2/F_2), (Y_1/F_2), and (Y_2/F_1). All other measurements must be derived from these four. Element (1,1) of equation (31) can be directly measured, and element (2,1) can be found using the rotational response technique of equation (29). Element (1,2) is given by:

$$\left(\frac{Y_2}{Q_1}\right) = \frac{1}{l_A}\left[\left(\frac{Y_2}{F_2}\right) - \left(\frac{Y_2}{F_1}\right)\right] \qquad (32)$$

since F_1 and Q_1 can be replaced with F_2 and $l_A F_2$ respectively to create the same response at Y_2 (Figure 6c). The right-hand side of equation (32) is made up entirely of direct experimental measurements. Similar strategies are applied to populate other matrices as summarized in Table 4. These matrices are placed into the decomposition equation (14).

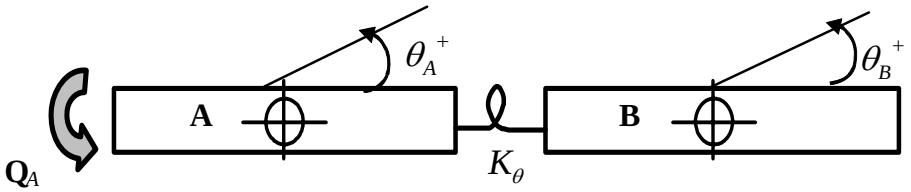

Fig. 5. Rigid components, A and B, joined by a rotational stiffness element K_θ.

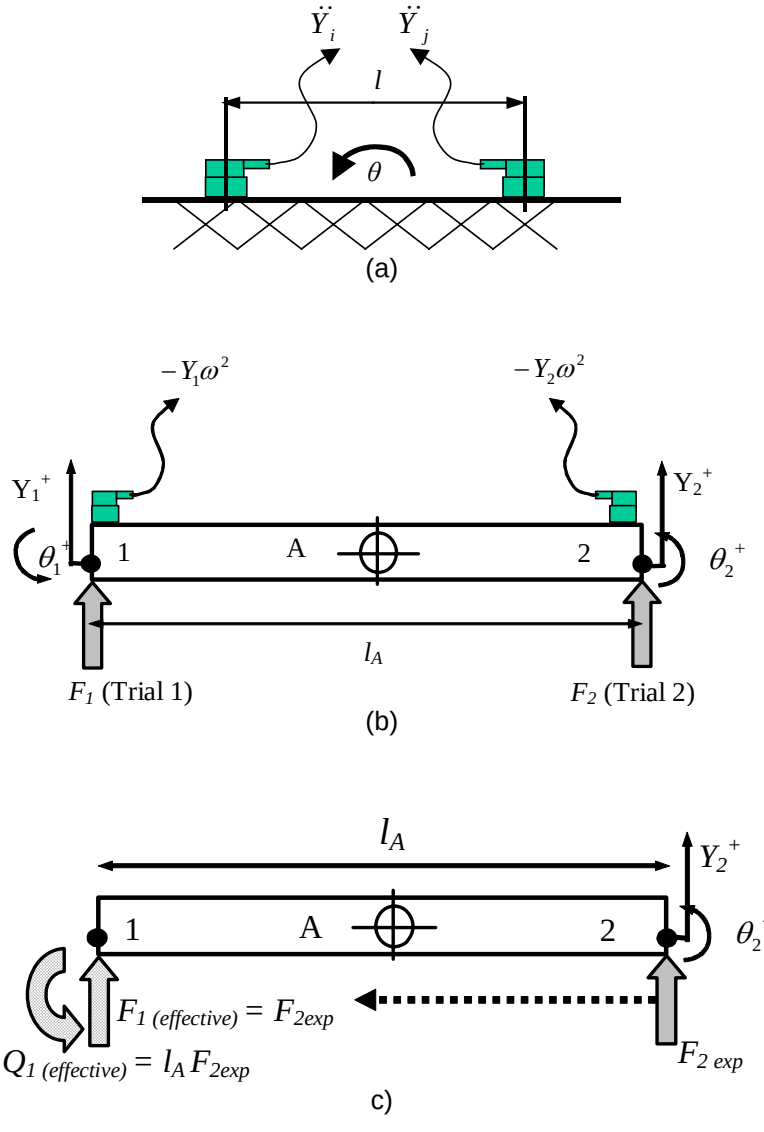

Fig. 6. Measurement of rotational response (a) Two accelerometer method, (b) Sign conventions for rigid mass A, (c) Generation of moment excitation using impulse hammer

$\boldsymbol{\alpha}_{21}(\omega)$	$\begin{bmatrix} \frac{Y_2}{F_1} & \frac{Y_2}{Q_1} \\ \frac{\theta_2}{F_1} & \frac{\theta_2}{Q_1} \end{bmatrix}_\omega$	$\begin{bmatrix} \left(\frac{Y_2}{F_1}\right) & \frac{1}{l_A}\left[\left(\frac{Y_2}{F_2}\right)-\left(\frac{Y_2}{F_1}\right)\right] \\ \left(\frac{\theta_2}{F_1}\right) & \frac{1}{l_A}\left[\left(\frac{\theta_2}{F_2}\right)-\left(\frac{\theta_2}{F_1}\right)\right] \end{bmatrix}_\omega$
$\boldsymbol{\beta}_{43}(\omega)$	$\begin{bmatrix} \frac{Y_4}{F_3} & \frac{Y_4}{Q_3} \\ \frac{\theta_4}{F_3} & \frac{\theta_4}{Q_3} \end{bmatrix}_\omega$	Same as α_{21} since components A & B are identical
$\boldsymbol{\alpha}_{22}(\omega)$	$\begin{bmatrix} \frac{Y_2}{F_2} & \frac{Y_2}{Q_2} \\ \frac{\theta_2}{F_2} & \frac{\theta_2}{Q_2} \end{bmatrix}_\omega$	$\begin{bmatrix} \left(\frac{Y_2}{F_2}\right) & \frac{1}{l_A}\left[\left(\frac{Y_2}{F_2}\right)-\left(\frac{Y_2}{F_1}\right)\right] \\ \left(\frac{\theta_2}{F_2}\right) & \frac{1}{l_A}\left[\left(\frac{\theta_2}{F_2}\right)-\left(\frac{\theta_2}{F_1}\right)\right] \end{bmatrix}_\omega$
$\boldsymbol{\beta}_{33}(\omega)$	$\begin{bmatrix} \frac{Y_3}{F_3} & \frac{Y_3}{Q_3} \\ \frac{\theta_3}{F_3} & \frac{\theta_3}{Q_3} \end{bmatrix}_\omega$	$\begin{bmatrix} \left(\frac{Y_3}{F_3}\right) & \frac{1}{l_B}\left[\left(\frac{Y_3}{F_4}\right)-\left(\frac{Y_3}{F_3}\right)\right] \\ \left(\frac{\theta_3}{F_3}\right) & \frac{1}{l_B}\left[\left(\frac{\theta_3}{F_4}\right)-\left(\frac{\theta_3}{F_3}\right)\right] \end{bmatrix}_\omega$
$\mathbf{H}_{41}(\omega)$	$\begin{bmatrix} \frac{Y_4}{F_1} & \frac{Y_4}{Q_1} \\ \frac{\theta_4}{F_1} & \frac{\theta_4}{Q_1} \end{bmatrix}_\omega$	$\begin{bmatrix} \left(\frac{Y_4}{F_1}\right) & \frac{1}{l_A}\left[\left(\frac{Y_4}{F_2}\right)-\left(\frac{Y_4}{F_1}\right)\right] \\ \left(\frac{\theta_4}{F_1}\right) & \frac{1}{l_A}\left[\left(\frac{\theta_4}{F_2}\right)-\left(\frac{\theta_4}{F_1}\right)\right] \end{bmatrix}_\omega$

Table 4. Strategy for populating the experimental compliance matrices (equation 14) that are experimentally determined.

Validation of Compliance Matrices

For experimental study, a frequency range from 0 to 500 Hz is chosen. The $\boldsymbol{\alpha}(\omega)$ (and similarly $\boldsymbol{\beta}(\omega)$) spectra verify that they indeed represent rigid bodies over the selected frequency range (Figure 7). Also, Figure 7 compares experimental (EXP) and lumped model (LPD) $\boldsymbol{\alpha}_{21}$ spectra based on the system described in Figure 2 and Table 1. The four sub-plots describe the four elements of the dynamic compliance matrix: $\boldsymbol{\alpha}_{X/F}, \boldsymbol{\alpha}_{X/Q}, \boldsymbol{\alpha}_{\theta/F}$ and $\boldsymbol{\alpha}_{\theta/Q}$. These represent components of displacement (*X*) or rotation (θ) due to force (*F*) or moment (*Q*). Only the spectra magnitude curves are shown, as they are representative of all $\boldsymbol{\alpha}$ and $\boldsymbol{\beta}$ spectra. Not only do the magnitudes correlate for all four elements of the $\boldsymbol{\alpha}_{21}$ matrix ($\boldsymbol{\alpha}_{X/F}, \boldsymbol{\alpha}_{X/Q}, \boldsymbol{\alpha}_{\theta/F}$ and $\boldsymbol{\alpha}_{\theta/Q}$), but their phases also match though not shown here. Since the experimental and simulated results match, analytical descriptions of A and B are employed for the decomposition procedure in all three sets of calculations LPD, FEM and EXP.

In the FEM model, harmonic analysis is used to obtain the FRF's for displacements at points 1, 2, 3 and 4 (Figure 2) given excitations at 1 and 2. The finite element model data are then processed to define the elements of $\mathbf{H}_{41}$

for the extraction of $\mathbf{K}_d(\omega)$ using FEM. The lumped simulation model (LPD) takes into account only the first two modes of the system, and therefore the modeling strategy may be a source of discrepancy between prediction and measurement.

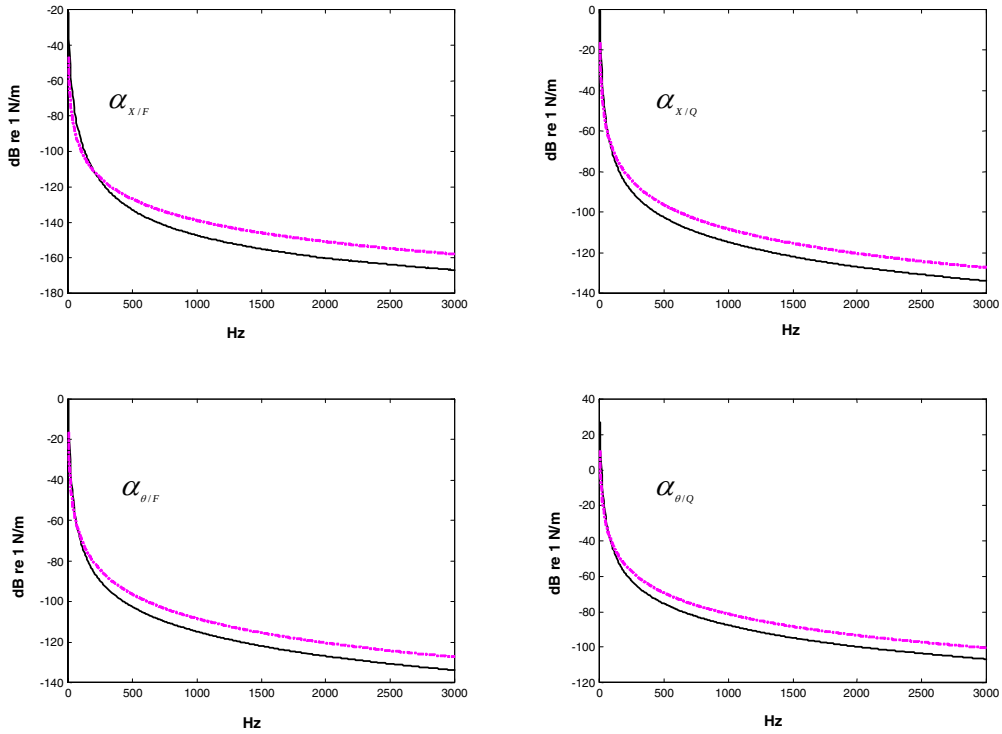

Fig. 7. Cross compliance α21 spectra. Key: ——Measurement (EXP); ----------Model (LPD)

RESULTS

Estimation of $K_d(\omega)$

Since all elements of the compliance matrices are frequency-dependent, the decomposition calculation of Figure 1 can be performed at any frequency, ω. For the simulation model, LPD, where the "input" beam stiffness $\mathbf{K}_{\mathbf{Euler}}$ is purely static according to Euler beam theory, the resulting "output" stiffness matrix $\mathbf{K}_{output} = \mathbf{K}_d(\omega) = \mathbf{K}_s(\omega)$ resulting from decomposition (14) would also be ideally independent of the frequency (ω) chosen for calculation. In other words, the spectrum of each stiffness element should be a horizontal line when plotted against frequency. Here, we choose to calculate $\mathbf{K}_d(\omega)$ with $\Delta\omega$ of 5 Hz for both the lumped model and the experiment but the resolution is 50 Hz for finite element calculations. Equation (19) can be partitioned into 4 sub-matrices as:

$$\mathbf{K}_S = \begin{bmatrix} [\mathbf{K}_I] & [\mathbf{K}_{II}] \\ [\mathbf{K}_{III}] & [\mathbf{K}_{IV}] \end{bmatrix} \tag{33}$$

This matrix is obtained for a beam element corresponding to translations (Y_1, Y_2) and rotations (θ_1, θ_2) at each end in response to applied force and moment if we assume the beam to be fixed at the other end. Rearrange the force-displacement equations to give the force and moment for relative displacement (Y_1-Y_2) and relative rotation (θ_1+θ_2), per the sign convention we have adopted. The stiffness matrix (2x2) for this is equal to K_{12} of equation (33).

In evaluating the $\mathbf{K}_d(\omega)$ spectra of the lumped model (LPD), several frequency peaks are observed in Figure 8 suggesting that $\mathbf{K}_d(\omega)$ acquires inertial properties during the decomposition process. Otherwise, the spectra would yield spectrally-invariant values. It appears that the peaks are related to the anti-resonances of the $\mathbf{H}_{41}$ spectra (Figure 9) and could result from numerical errors associated with matrix inversion. When the decomposition procedure is analytically processed, the $\mathbf{K}_d(\omega)$ matrix shows the nature of each element with respect to ω. The analytical expression for $\mathbf{K}_d(\omega)$ shows that all elements of the matrix take the following form where $\mathbf{K}_{ij}$ are the elements of 2x2 dynamic stiffness matrix. Here, *i* and *j* imply the *F/X*, θ/X, F/θ and Q/θ terms.

$$\mathbf{K}_{ij} = \frac{b_4(i,j)\omega^4 + b_2(i,j)\omega^2}{a_4\omega^4 + a_2\omega^2 + a_0} \tag{34}$$

The values of $b_4(i,j)$ and $b_2(i,j)$ depends on *i* & *j* but a_4, a_2 and a_0 are the same for a particular joint. The above expression clearly shows presence of poles and zeros in the stiffness spectra which are obtained both experimentally (EXP) or theoretically (LPD or FEM).

At higher frequencies, the asymptote of each stiffness spectrum approaches the absolute value of the top-right and bottom-left quadrants of $\mathbf{K}_{Euler}$ as shown in Figure 8. This indicates that the "output" stiffness matrix of dimension 2 may best represent the cross-point stiffness quadrants. The asymptotic trends of extracted stiffness terms match EXP, LPD and FEM spectra well with the exception of $K_{Q\theta}$.

Comparison of $K_d(\omega)$

When the $\mathbf{K}_d(\omega)$ matrix from lumped model (LPD) is compared (Fig. 8) with those derived from the finite element model (FEM) and experiment (EXP), we see that FEM and EXP do not always match LPD at the higher frequencies. This is probably related to the fact that FEM and EXP include high frequency modes in the data, while LPD contains only two non-zero modes (Table 2). It is shown, however, that FEM, LPD, EXP tend to converge to the K_{Euler} values from the beam stiffness matrix.

Below the second natural frequency, the correlation between three methods depends on the nature of the matrix element. Notice that a much stronger correlation is seen between EXP and FEM for those elements that are derived from the measurement of translational displacements ($K_{F/X}$ and $K_{Q/X}$). For elements related to the measurement of rotational displacements ($K_{F/\theta}$ and $K_{Q/\theta}$), a weaker correlation between EXP and FEM is found. This is due to the increased measurement error in the rotational displacement concept based on taking a difference between measured accelerometer signals.

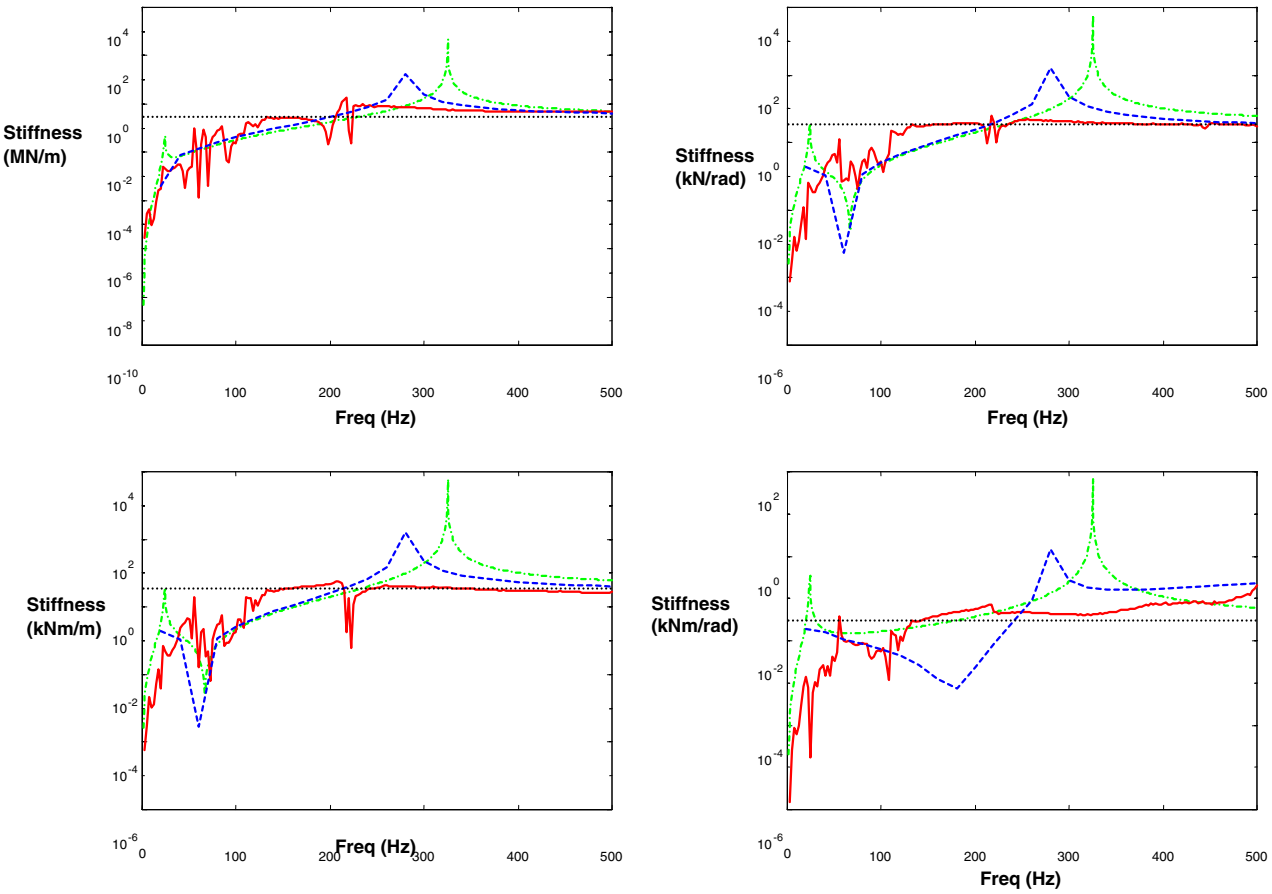

Fig. 8. Static stiffness spectra results of decomposition.
Key: Measurement (EXP); (LPD); Finite Elements (FEM); Expression (K_{Euler})

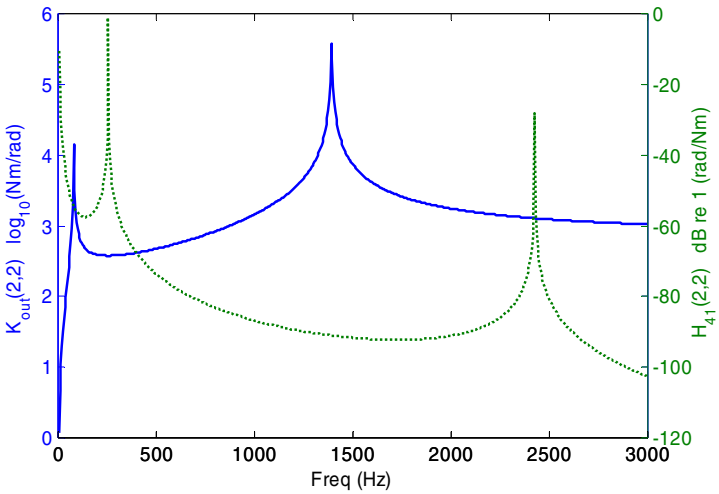

Figure 9. K_d calculated stiffness spectra with respect to H_{41} compliance for element (2,2) of both matrices. This is representative of all K_d elements. (Data shown is based of a test case with different physical dimensions than that shown in Table 2.) Data is based on the lumped model (LPD). Key: ——— K_d, ····· H41

CONCLUSION

This study demonstrates that an elastic beam joint can be described by a multi-dimensional lumped stiffness matrix for the first two assembly modes. The joint stiffness matrix is found from a decomposition technique based on the frequency domain component synthesis method. The method enables the extraction of diagonal as well as off-diagonal stiffness terms with data derived from lumped models (LPD), finite elements (FEM), and experimental measurement (EXP). The results are compared with static stiffness calculations based on Euler's beam theory-based. Natural frequencies resulting from the Euler beam lumped assembly model match measured values within 10%.

Unlike some methods proposed in the literature, our study uses only FRF's obtained under free-free boundary conditions. A laboratory test system with an elastic beam joint may be represented by a lumped joint (of dimension 2) with rotational and shear degrees of freedom. An analytical model based on the Euler beam theory (LPD) is successfully processed through the decomposition. The resulting joint dynamic stiffness spectra do, however, show some peaks that appear to line up with anti-resonant frequencies of assembly. Our analytical work explains the presence of poles and zeros in the stiffness frequency spectra. Future work should carefully examine and attempt to overcome the errors introduced by the matrix inversion process with techniques such as Singular Value Decomposition as suggested by Gialamas and Tsahalis [27].

The particular case studied in this article has addressed a simple problem of an elastic beam joint. Sheet metal structures with welded joints are similar. Extensions of this work have been reported by Mehta and Singh [28, 29]. To make the technique more robust, the effect of boundary conditions posed by welded or alternative joints must be studied. Also, a combination of experimental and theoretical decomposition methods should be studied within the context of practical structures given a wide assortment of joints. Multiple joint cases need to be addressed in future research. The extraction of joint damping is yet another important issue for adhesive joints or structural glues. Finally, improving the measurement of rotational displacements is a vital area for further work in this area. The application of a laser Doppler vibrometer to measure rotational displacements on assemblies with compliant components might be useful.

ACKNOWLEDGEMENTS

We gratefully acknowledge the financial support from the Edison Welding Institute (www.ewi.org) and J. Crompton for suggestions.

REFERENCES

[1] Ren Y, Beards CF. On the Nature of FRF Joint Identification Technique. Proceedings of the 11th International Modal Analysis Conference 1994; 1 (of 2): 473-478.

[2] Kamal M, Wolf J. Modern Automotive Structure Analysis. Van Norstrand Reinhold Company, 1982; 116-194.

[3] Rediers B, Yang B, Juneja B. Static and Dynamic Stiffness - One Test, Two Results. Sound and Vibration August,1998; 22-24.

[4] Wang JH, Liou CM . Experimental Identification of Mechanical Joint Parameter. ASME Journal of Vibration and Acoustics 1991;113: 28-36.

[5] Ren Y, Beards CF. On the Importance of Weighting for FRF joint identification. Proceedings of the 11th International Modal Analysis Conference 1993; 1(of 2): 1606-1611.

[6] Ren Y, Beards CF. A Iterative Joint Identification Technique. Proceedings of the 11th International Modal Analysis Conference 1993; 1(of 2): 1133 –1139.

[7] Juanxin Su, Mak CM. Direct Measurement of Moment Mobility and a Moment Excitation System. Applied Acoustics 2002;63 139-151.

[8] Ivarsson LH; Sanderson MA, MIMO Technique for Simultaneous Measurement of Translational and Rotational Mobilities, Applied Acoustics 2000;61 345-370.

[9] Liu W, Ewins DJ. Substructure Synthesis via Elastic Media. Part I: Joint Identification. International Modal Analysis Conference 2000; 1153-1159.

[10] Liu W, Ewins DJ. Substructure Synthesis via Elastic Media. Part II: Joint Identification . International Modal Analysis Conference 2000; 1160-1165.

[11] Chen SY, Ju MS, Tsuei YG. Estimation of Mass, Stiffness and Damping Matrices from Frequency Response Functions. Journal of Vibration and Acoustics 1996;118, 78-82.

[12] Tsai JS, Chou YF. The Identification of Dynamic Characteristics of a single bolt joint. Journal of Sound and Vibration 1998;125(3):487-502.

[13] Liu W, Ewins DJ. The Importance Assessment of RDOF in FRF Coupling Analysis. website: http://www.me.ic.ac.uk/dynamics /publication/external/ other/ WL_IMAC17.pdf

[14] Stainbridge A, Ewins DJ. Measurement of Translational and Angular Vibration using a Scanning Laser Doppler Vibrometer. Shock and Vibration Digest 1996; 3:141-152.

[15] Mitchell LD, West RL, Wicks WL. Test Data Measurement – A Future Vision. Proc. IUTAM-IITD International Winter School on Optimum, Dynamic Design, New Delhi, India 1997.

[16] Yoshimura T, Hosoya N. FRF Estimation on rotational Degrees of Freedom of Structures. International Modal Analysis Conference 2000; 1667-1671.

[17] Singh R, Liaw ML, Farstad JE, Kung SW. Determination of Joint Stiffness through Vibration Analysis of Beam Assemblies. Edison Welding Institute Research Report 1995; MR9502.

[18] Liu Y, Lim. TC, Wang, Y. Vibration Characteristics of Welded Beam and Plate Structures. Noise Control Engineering Journal 2001; 49 (6): 265-275.

[19] Bishop RED, Johnson DC. The Mechanics of Vibration 1960. Cambridge: Cambridge University Press.

[20] Snowdon JC. Mechanical Four-Pole Parameters and Their Application. Journal of Sound and Vibration 1971; 15(3): 307-323.

[21] Soedel W. Vibrations of Shells and Plates 1981. New York: Marcel Dekker, Inc.

[22] Rook TE, Singh R. Mobility Analysis of Structure-borne Noise Power Flow through Bearings in Gearbox-like Structures. Noise Control Engineering Journal 1996; 44(2): 69-78.

[23] Sykes AO. 1968. Development and Application of Linear Multi-Terminal Network Theory to Vibration Problems. Ph.D. Thesis, The Catholic University of America, Washington D. C., USA

[24] Thomson WT. Theory of Vibration With Applications 1993; Prentice Hall, 4th ed. 179-180, 306-309.

[25] ANSYS Inc. version 5.7, Canonsburg, Pennsylvania, USA.

[26] Ewins DJ. Modal Testing: Theory and Practice. Research Studies Press 1984; 146-148.

[27] Gialamas TP, Tsahalis DT. Substructuring Technique: Improvement by Means of Singular Value Decompositions (SVD). Applied Acoustics, 2001; 62, 1211-1219.

[28] Mehta P, Singh R. Estimation of Dynamic Stiffness Matrix of Welded or Glued Joints Using Laboratory Fixture. SAE, 2003. Paper # 03NVC-252.

[29] Mehta P, Singh R. Effect of Welded or Glued Joints on Modal Properties of an Assembly. SAE, 2003. Paper # 03NVC-253.